Article

Design of magneto-inductive waveguide in 2-d magnetic metamaterial structure for wireless power transfer and near-field communications

Xuan Thanh Pham[1], Xuan Hung Nguyen[1], Kim Hoan Vu[1], Dinh Linh Trinh[2], Thanh Son Pham[1,*]

[1] Faculty of Electronics Engineering, Hanoi University of Industry, Hanoi 11900, Vietnam
[2] Institute of System Integration, Le Quy Don Technical University, Hanoi 11900, Vietnam
* Corresponding author: Thanh Son Pham, sonpt@haui.edu.vn

Abstract: Recently, significant research has been conducted on magnetic metamaterials that exhibit negative permeability and operate within the GHz and MHz frequency ranges. These metamaterial structures can be utilized to improve the efficiency of near-field wireless power transfer systems, subterranean communication, and position sensors. However, in most cases, they are only designed to work for a single application. This study focuses on examining the transmission of magneto-inductive waves in magnetic metamaterial structures with ordered arrangements. This structure can be used simultaneously for wireless power transfer and near-field communications. The unit cell is formed by a spiral with five turns that is implanted on a FR-4 substrate. An external capacitor was used to regulate the resonant frequency of the magnetic metamaterial unit cell. The properties of magneto-inductive waves, including reflection, transmission response, and field distribution on the waveguide, have been extensively computed and simulated. The obtained results indicate that both 1-dimensional and 2-dimensional magnetic metamaterial configurations possess the ability to conduct electromagnetic waves and propagate magnetic field energy at a frequency of 13.56 MHz. The straight and cross path configurations were also investigated to identify the optimal configuration on the 2-dimensional metamaterial slab.

Keywords: magnetic metamaterial; magneto-inductive; waveguide; wireless power transfer; near-field communications

1. Introduction

Metamaterials are artificially engineered composite structures that exhibit unique electromagnetic properties not present in conventional materials. In 1968, Victor Veselago introduced the notion of metamaterials by conducting a theoretical examination of substances that exhibit negative values for both permittivity (ε) and permeability (μ) simultaneously [1]. In 1996 and 1999, John Pendry published two articles demonstrating the first practical metamaterial implementation. These studies introduced the concepts of negative permittivity utilizing wire structure and negative permeability using split ring medium, marking a significant milestone after 30 years of anticipation [2,3]. Metamaterials exhibit various unique phenomena that are not found in natural materials, including evanescent wave amplification, backward wave propagation, inverse Doppler effect, negative Goos-Hanchen shift, and backward Cerenkov radiation [4–7]. Metamaterials can be applied in the domains of energy harvesting [8,9], perfect absorbers [10,11], and boosting antenna efficiency [12] due to their unique features.

Materials can be categorized into four classes based on their permittivity and permeability values: double-positive, epsilon-negative, double-negative, and mu-

negative [13,14]. Understanding the distinct properties and applications of these four classes of materials is crucial for advancing research and development in fields such as material science, engineering, and applied physics. Double-positive materials are those that naturally occur and exhibit both positive permittivity and permeability. These materials are commonly found in nature and are not engineered or synthesized. On the other hand, epsilon-negative and double-negative materials are typically composite materials that are specially engineered to exhibit unique electromagnetic properties. These materials primarily operate in the GHz (gigahertz) and THz (terahertz) wavelength regions, making them suitable for advanced technological applications such as telecommunications and imaging systems [15–18]. These metamaterials have garnered significant interest in recent years due to their potential applications in creating novel devices like cloaking devices, superlenses, and advanced antenna systems [19,20].

Mu-negative materials, commonly referred to as magnetic metamaterials, are distinctive due to their unique property of negative magnetic permeability. Unlike other categories of materials, where multiple aspects might be considered, mu-negative materials are exclusively focused on their magnetic properties. This singular focus enables them to interact with magnetic fields uniquely and remarkably. Operating primarily within the MHz frequency range, magnetic metamaterials have garnered significant attention for their extensive applications in wireless power transfer (WPT) and near-field communication systems [21–24]. These magnetic metamaterials are compatible with supporting slow-propagating waves, known as magneto-inductive waves (MIWs) [25]. These waves arise from the intricate inter-element connections among the regularly arranged unit cells within the metamaterial's structure. The unique ability of mu-negative materials to support MIWs facilitates efficient energy transfer and enhances communication capabilities over moderate distances. This makes them indispensable in the realm of modern technological applications, ranging from consumer electronics to advanced communication systems [26,27].

WPT has emerged as a pioneering technology that has undergone extensive research and development in recent years [28–31]. One of the critical factors influencing the performance of WPT systems is the transmission distance. When the transfer distance increases, the efficiency of the WPT system reduces significantly. To address this challenge, magnetic metamaterials are employed due to their ability to amplify evanescent waves in the near field [32,33]. This amplification helps to enhance the performance of WPT systems. Moreover, magnetic metamaterials possess a unique characteristic of having a negative permeability region at resonant frequencies. This particular property makes them ideal for propagating MIWs in the MHz frequency range [34,35]. These MIWs exhibit unique behaviors, such as a negative dispersion curve for backward propagation and the creation of sub-wavelength waveguides. The distinct properties of magnetic metamaterials open up various advanced applications, including enhancing WPT systems [36]. The magnetic metamaterial structure, capable of being rolled and folded, has been applied to enhance the performance of WPT systems, increasing the distance and optimizing the transmission space. The bending metamaterial slab with a cavity structure can localize

the magnetic field into the desired spatial region, thereby improving safety and minimizing losses in the system [37–39].

This study focuses on examining the transmission of MIW in ordered magnetic metamaterial structures. The unit cell is composed of a spiral resonator that is supported by an external capacitor to adjust the resonant frequency to resonate at around 13.56 MHz. The properties of MIW, such as reflection, transmission response, and field dispersion, have been extensively computed and simulated. The outcome indicates that MIW is capable of propagating through a 1-dimensional (1-D) metamaterial array consisting of 9 elements, with a transmission coefficient of −12 dB at a frequency of 13.56 MHz. Several metamaterial configurations are also investigated in 2-dimensional (2-D) for propagating the magnetic energy by MIW. This metamaterial structure can be utilized for WPT and near-field communication in environments with high levels of signal loss for far-field antennas. Furthermore, the proposed magnetic metamaterial structure has significant potential for utilization in magnetic resonance imaging (MRI), near-field focusing, sub-wavelength waveguide devices, and MIW components.

2. Design of magnetic metamaterial unit cell

Multiple methods exist for constructing a magnetic metamaterial that operates within the low-frequency range, such as low GHz or MHz. The combination of a split-ring resonator with an external lumped capacitor is an effective method for creating a magnetic metamaterial structure [40]. **Figure 1a** depicts a schematic of a unit cell of a magnetic metamaterial. The unit cell comprises a 5-turn spiral resonator (5T-SR) that is equipped with a lumped capacitor. The 5T-SR possesses a planar configuration, which facilitates its fabrication and integration into electrical systems. The 5T-SR in this study is characterized by a circular shape of 5 cm in length, a strip width of 1.5 mm, and an inter-strip spacing of 1.5 mm. The FR-4 substrate has a thickness of 1.2 mm, a dielectric constant of 4.4, and a copper thickness of 0.035 mm. In order to adjust the resonant frequency of the 5T-SR, an external capacitor is connected across the two terminals of the metal strip of the spiral resonator. The capacitor installed at this location is regarded to be connected in parallel with the internal capacitor of the spiral [41]. The unit cell was designed for the fabrication process using a printed circuit board (PCB) technique with a resolution of 0.1 mm to minimize error and high scalability. In designing this magnetic metamaterial configuration, it is essential to consider the following criteria: (i) select an appropriate metamaterial slab size based on the application conditions; (ii) optimize the number of turns, inner radius, and width of the coils to achieve maximum efficiency for the unit cell while maintaining a fixed size; and (iii) recognize that the choice of materials for the spiral and the substrate will influence losses within the structure, while also taking material costs into account.

Figure 1b illustrates the simple electrical model of the 5T-SR. Here, L_0 refers to the self-inductance of the 5T-SR, with a spiral structure consisting of 5 coils. The coil's inductance is much higher than a loop of the same size. Hence, the quality factor (Q-factor) of the resonator coil has a very high value. C_{gap} refers to the self-capacitance of the 5T-SR. This value is quite small, so the natural resonant frequency of the coil is often quite high, and C_0 represents the capacitance of the additional capacitor to lower

the resonant frequency of the coil to the desired frequency region. The operating frequency of the unit cell can be adjusted by choosing the appropriate capacitance for the external capacitor. Ohmic losses can be represented by a series resistor, denoted R_0. From the above elements, the 5T-SR shown in **Figure 1a** has been modeled into a resonant circuit, as shown in **Figure 1b**.
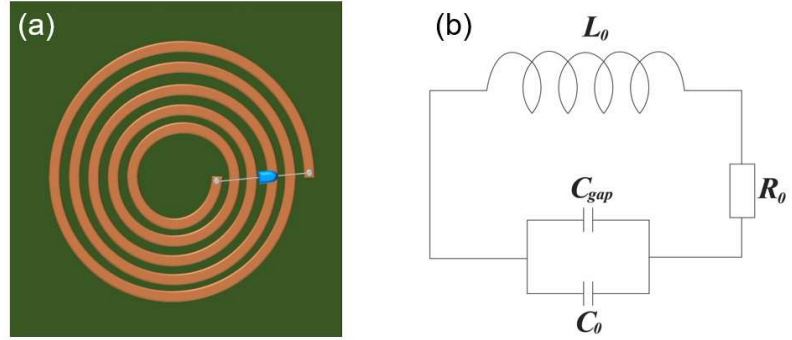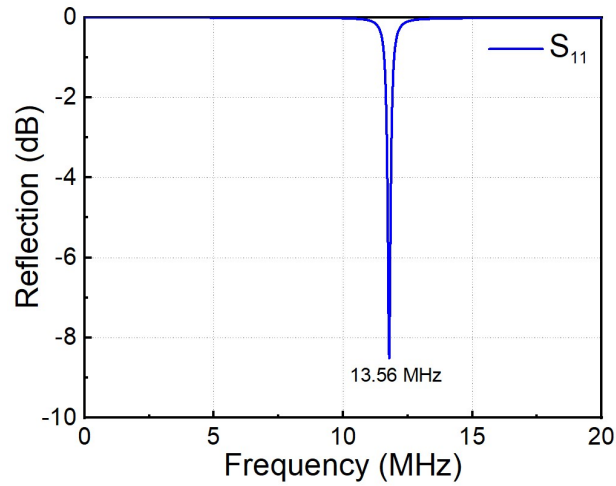

Figure 1. (a) Magnetic metamaterial unit cell with an external capacitor; **(b)** equivalent circuit model of the unit cell.

From the electrical model of 5T-SR in **Figure 1b**, the resonant frequency of the metamaterial unit cell can be given by:

$$f = \frac{1}{2\pi\sqrt{L(C_{gap} + C_0)}} \tag{1}$$

Electromagnetic (EM) simulations are used to study the properties of metamaterial unit cells. The simulation was performed using the CST Studio Suite program. The simulation includes appropriate boundary conditions for the waveguide containing the 5T-SR; open boundary conditions for all directions were used in this simulation. In the simulation, a metamaterial unit cell is set between two ring antennas linked to two virtual ports, and the distance between the antennas and the 5T-SR is adjusted so that the lowest insertion loss value can be obtained from 5T-SR at the resonant frequency. **Figure 2** shows the reflectivity of the metamaterial unit cell when a mount capacitor with a capacitance value of 145 pF is used. The results indicate that the metamaterial unit cell exhibits resonance at a frequency of 13.56 MHz. The high sharpness of the resonance dip presents that the unit cell possesses a very high Q-factor capable of reducing intrinsic losses, which is very suitable for WPT. The resonant frequency of the unit cell can be easily controlled by external capacitors; therefore, the unit cell structure has the capability to apply in multi-frequencies systems or switching. A negative permeability was observed in metamaterial structures at frequencies higher than the resonant frequency of metamaterial unit cells in Ref. [40]. By using the negative permeability range, evanescent amplification and backpropagation of the MIW can be realized.

Figure 2. The reflection response of magnetic metamaterial unit cell.

We create a waveguide by assembling magnetic metamaterial unit cells on a 2-D metamaterial array. **Figure 3** depicts the proposed 2-D magnetic metamaterial slab, including a total of 81 unit cells arranged in a 9 × 9 grid. The slab size is 45 × 45 cm. The waveguide is formed by using external capacitors with different values for the waveguide and the rest of the metamaterial slab. The waveguide in this setup has a capacitor value of 145 pF, as shown in **Figure 1**. The remaining portion of the metamaterial slab is equipped with a 185 pF capacitor. The unit cells have two distinct resonance frequencies of 13.56 MHz and 12.28 MHz, respectively. The unit cell's resonant frequency in the waveguide is 11% greater than that in the remainder of the metamaterial slab, causing the waveguide mode to fall within the hybridization bandgap of the slab [42]. Therefore, the magnetic field will be confined to the unit cells in the waveguide. The confinement of the MIWs in the waveguide region is a result of the hybridization band gap generated in the metamaterial slab. Thus, MIWs can be efficiently propagated in the waveguide. The waveguide configuration can be easily changed by adjusting the capacitance of the metamaterial unit cells. These MIW waveguides can be used in planar WPT or near-field communications.
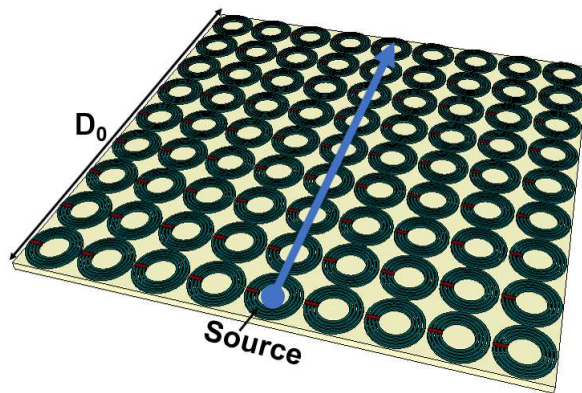
Figure 3. Schematic of 2-D magnetic metamaterial slab for magneto-inductive waveguiding.

The working principle of MIW devices is based on the propagation of magnetic fields through an array of coupled resonant elements. The devices can be used to

propagate the power and information. In some special environments, such as underground or under waves where the far-field electromagnetic devices suffer a large loss, those devices are very useful. The MIW devices are also applied to enhance or concentrate the magnetic field to improve the performance of the WPT system. MIW is also used to increase the signal-to-noise ratio in MRI systems. This principle allows for innovative designs in electromagnetic wave manipulation and transmission, particularly in miniaturized and integrated systems. The applications of MIW devices are diverse and impactful. In sensing technologies, these devices can facilitate the detection of various physical parameters by leveraging their unique propagation characteristics. Additionally, MIW devices are being explored for communication systems, providing innovative solutions for data transmission in compact and integrated forms. Their ability to manipulate electromagnetic waves makes them valuable in advancing modern technologies across multiple fields.

3. Results and discussions

We are examining a waveguide that is made up of a series of magnetic metamaterial unit cells. **Figure 4a** depicts the diagram of a resonator-coupled 1-D metamaterial array. The unit cells are separated by a distance of a and have a coupling coefficient of κ. In order to streamline the analysis, we focus solely on the interaction occurring between the closest neighboring elements. When the initial element is stimulated, MIWs propagate across the array. The present input of the nth unit cell can be represented as:

$$I_n = I_0 \, exp(-jkna) \tag{2}$$

where I_0 is the current of the first cell, $k = \beta - j\alpha$ is the wavenumber, β is the propagation constant, and α is the attenuation per length. The relation between β and ω gives the dispersion relation as:

$$\beta = \frac{1}{a} arccos\left(\frac{\omega_0^2/\omega^2 - 1}{\kappa}\right) \tag{3}$$

For a given Q-factor, α can be expressed as:

$$\alpha a = \frac{1}{\kappa Q \, sin(\beta a)} \tag{4}$$

In order to examine the electromagnetic characteristics of the waveguide, we conduct a simulation to gain a deeper understanding of its construction. **Figure 4b** illustrates the spatial distribution of the electromagnetic field in a 9-resonator array, which formed a waveguide. The magnetic field is confined within the waveguide and exhibits a high degree of concentration near the center of the 5T-SR. The field intensity decreases when the unit cell is located far from the source due to the attenuation on each metamaterial unit cell. The magnetic metamaterial array demonstrates the capability to transmit MIW within the structure through the use of both electrical models and field analysis. That type of MIW operates at a low MHz frequency and mostly propagates along the surface of the magnetic metamaterial slab. In this configuration, the incident wave is excited by a loop antenna placed near the first unit cell of the metamaterial array. The alternative current resonates at 13.56 MHz in the

loop antenna and induces a current in the first unit cell. Through coupling between unit cells, the current from the first unit cell can induce the currents in the sequence unit cell. Thanks to that, the MIW can be propagated. MIW only propagates magnetic energy, so it is non-polarized. One important point to highlight is that, as both the antenna and all unit cells operate within the near-field region in the subwavelength regime, the waves propagating in this scenario are non-polarized and do not exhibit the incident angle as electromagnetic wave propagation in the far-field. However, for effective coupling between the antenna and the unit cell, the magnetic field generated by the antenna must be perpendicular to the surface of the unit cell. In other words, the surface of the antenna should be parallel to the surfaces of the unit cells.

In this proposed metamaterial structure, unit cells with a size of $a = 5$ cm are employed. The Q-factor of each unit cell has been calculated to be 150. The coupling coefficient between consecutive unit cells within the waveguide, spaced 5 cm apart, is calculated to be $\kappa = 0.036$. Consequently, applying Equation (4), we determine that the minimum attenuation coefficient at the resonant frequency of the unit cell within the waveguide reaches a value of $\alpha = 0.011$/cm. The concentration of magnetic field in the metamaterial unit cell may cause an increase in temperature. In this metamaterial structure, which consists of cooper layers on the FR-4 (Fire Retardant) substrate, the performance of metamaterials is not sensitive to temperature. Of course, with too high temperatures, the conductivity of the cooper is reduced, leading to an increase in the resistance of the unit cell, which degrades the efficiency of the system. The substrate loss also affects the performance of the metamaterial slab. Factors such as material and thickness will influence the Q-factor of the unit cell. However, the FR-4 substrate used in this case has been optimized for a balance between loss and cost. Substrate loss in the MHz frequency range does occur; however, it is considerably much lower than in the GHz frequency range.
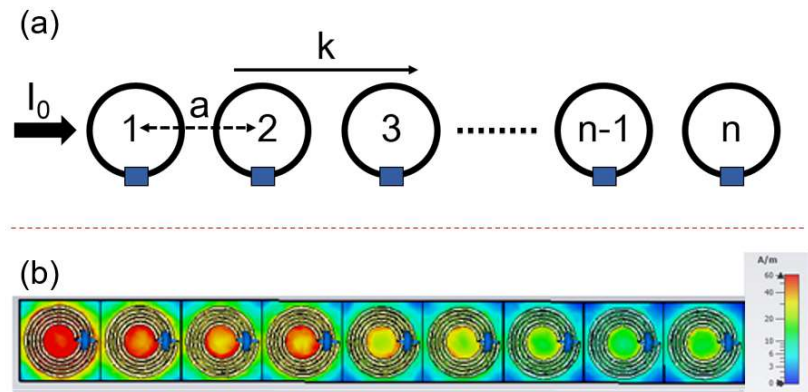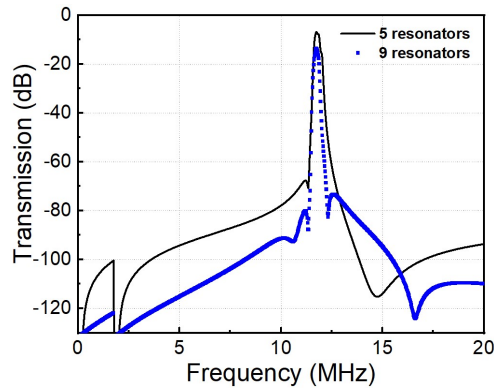

Figure 4. The 1-D magnetic metamaterial array. **(a)** The schematic of 1-D magnetic metamaterial array. **(b)** Magnetic field distribution in metamaterial array.

Figure 5 illustrates the transmission coefficient of MIW in the one-dimensional metamaterial arrays. To obtain the transmission of the metamaterial array, we used two ports simulation to analyze the structure. The excitation port is connected to a loop antenna placed near the first unit cell as a transmitter. Another port and antenna are placed close to the unit cell at the end of the array. All the boundary conditions are set as "open". The transmission peak is observed at −6 dB (black-line curve) and −12 dB

(blue-dot curve) at a frequency of 13.56 MHz. This occurs when there are 5 and 9 resonators, respectively. Due to the fact that the MIW is a surface wave that propagates on the metamaterial slab within the low MHz frequency range, the loss of radiation can be disregarded. The reduction in MIW intensity can be attributed to the Ohmic loss occurring in the unit cells of the metamaterial. The loss is attributed to attenuation, as explained in Equation (4) in relation to the *Q*-factor. The *Q*-factor of the unit cell obtained from the simulation is 150. The transmission bandwidth is 402 kHz for the 5-resonator waveguide and 368 kHz for the 9-resonator waveguide. The aforementioned results indicate that a metamaterial chain consisting of either 5 or 9 5T-SR units is capable of facilitating WPT. However, it is important to note that the system's performance significantly degrades as the length of the waveguide increases. Furthermore, MIWs can be effectively utilized for signal transmission within the MHz frequency range, offering bandwidths exceeding 300 kHz.

**Figure 5.** Transmission coefficient of 1-D metamaterial array.

It is simple to expand the 1-D array into a 2-D metamaterial slab. **Figure 6** displays the spatial distribution of the electromagnetic field within the waveguide in the metamaterial slab. The resonance frequency of all the cells located at the middle of the vertical axis in the metamaterial slab is altered in order to establish the waveguide. We saw clearly defined and powerful fields confined within the waveguide. The MIW is propagating in the waveguide direction, analogous to the scenario of a 1-D metamaterial array. Due to the intense field confinement in the waveguide, the *Q*-factor of the unit cell is higher in the waveguide compared to the 1-D array. The resonance frequency of a metamaterial unit cell can be adjusted by altering the capacitance of an additional capacitor by electrical means. Therefore, the waveguide configuration can be formed at many locations within a 2-D slab. Energy or signal can propagate via the waveguide from a single source to any location inside the metamaterial slab.
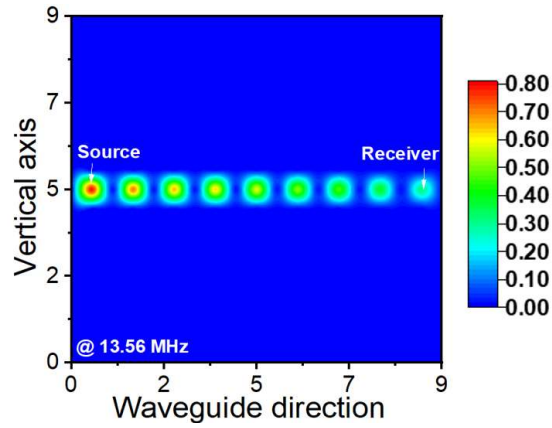
Figure 6. Field intensity on the metamaterial slab for MIW in a straight configuration.

In addition to the straight configuration illustrated in **Figure 6**, MIWs can also propagate through a slab metamaterial arranged in a diagonal configuration, as shown in **Figure 7**. The Q-factor of the unit cell in this diagonal configuration remains identical to that in the straight configuration. However, due to the increased distance within the diagonal arrangement, the attenuation coefficient of the MIW waveguide in the cross configuration is significantly larger compared to the straight configuration. Despite this increased attenuation, the cross configuration offers the flexibility to create various paths on the metamaterial, allowing MIWs to propagate to any point on the metamaterial slab efficiently.
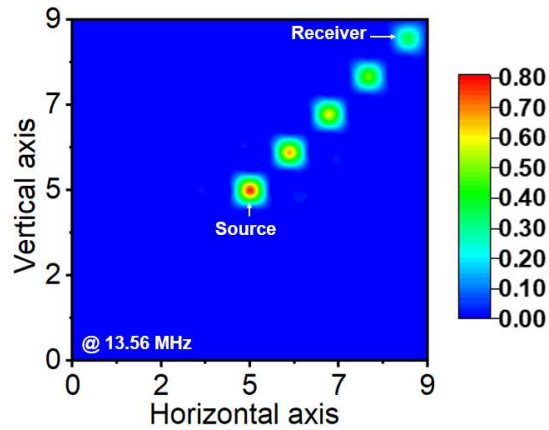
Figure 7. Field intensity on the metamaterial slab for MIW in a cross configuration.

Backward propagation is a distinctive feature of the MIW as it traverses the magnetic metamaterial waveguide. This phenomenon is illustrated in **Figure 8**, which presents the dispersion curve of the waveguide with a downward slope. The negative nature of the MIW is highlighted, where the phase velocity travels in the opposite direction to the energy velocity. This unique property is attributed to the negative coupling coefficient between adjacent metamaterial unit cells. In a planar arrangement, the magnetic field generated by the source metamaterial unit cell must change its direction to transfer energy to neighboring cells. The dispersion relationship further presents the ability of a metamaterial waveguide to transmit a slow wave, underscoring its potential in advanced waveguide applications.

In greater detail, backward propagation within the MIW is a fascinating attribute that distinguishes it from conventional wave behaviors. As depicted in **Figure 8**, the dispersion relation curve of the waveguide offers a visual representation of this complex phenomenon. What makes MIW particularly intriguing is its retrograde nature—here, the phase velocity, which represents the speed at which the phase of the wave propagates, moves in a direction opposite to that of the energy velocity, which is the rate at which energy is transmitted through the waveguide. This counter-intuitive motion is a direct consequence of the negative coupling coefficient found between adjacent metamaterial unit cells. The negative coupling coefficient plays a crucial role in this process. In a planar configuration, when a source metamaterial unit cell generates a magnetic field, this field must reverse its direction to facilitate energy transfer to neighboring cells. This directional change is essential for maintaining the backward propagation characteristic of MIW. Such behavior is not merely an academic curiosity but has practical implications as well.
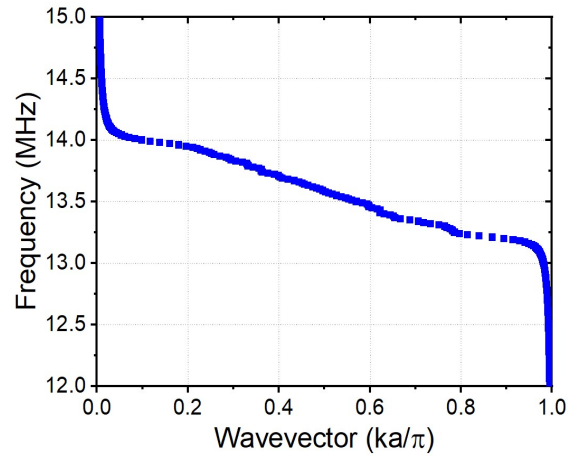
Figure 8. Dispersion relationship of the magneto-inductive waveguide in metamaterial structure.

The dispersion relationship provides deeper insights into how a metamaterial waveguide can effectively transmit slow waves. Slow waves are kind of waves that travel at speeds significantly lower than the speed of light in a vacuum, and their controlled transmission through a waveguide opens up numerous possibilities for advanced applications. These could range from enhanced signal processing capabilities to more sophisticated communication systems that leverage the unique properties of metamaterials.

In summary, the backward propagation of MIW within metamaterial waveguides is a unique and complex phenomenon driven by negative coupling coefficients and directional changes in magnetic fields. The ability to transmit slow waves further enhances the potential applications of these advanced waveguides, making them a promising area of study and innovation in modern physics and engineering. Despite the numerous strengths and advancements presented in this study, the magnetic metamaterial under investigation exhibits areas that need further examination and enhancement. One significant aspect is the reduction of the unit cell size, which would subsequently decrease the overall dimensions of the metamaterial slab. This reduction

must be achieved while maintaining the Q-factor to prevent an increase in losses associated with each unit cell, thereby preserving the system's performance. Addressing this challenge will be a focal point in our future research, thereby finding more applications for the proposed magnetic metamaterial configuration.

4. Conclusion

This study presents calculation and simulation results on the propagation of surface waves in a two-dimensional array of magnetic metamaterials, known as magneto-inductive waves. The MIW can be transmitted via negative magnetic coupling between metamaterial unit cells. An investigation has been conducted on the characteristics of MIW, including magnetic field dispersion, backward propagation, and attenuation. The magnetic metasurface being proposed operates within the MHz frequency band and experiences minimal radiation loss. Hence, it can be utilized in diverse subterranean and subaqueous communication scenarios where the installation of conventional communication links with far-field antennas is challenging due to radiation attenuation. The 2-D metamaterial slab is utilized in several fields, such as planar WPT, magnetic resonance imaging (MRI), near-field focusing, magneto-inductive wave devices, simultaneous power and data transfer, and subwavelength waveguide components.

Author contributions: Conceptualization, XTP and TSP; methodology, XHN; software, KHV; validation, KHV, DLT and XTP; formal analysis, DLT; investigation, XTP; resources, TSP; data curation, XHN; writing—original draft preparation, XTP; writing—review and editing, TSP; visualization, KHV; supervision, TSP; project administration, XTP; funding acquisition, XTP. All authors have read and agreed to the published version of the manuscript.

Conflict of interest: The authors declare no conflict of interest.

References

1. Veselago VG. The Electrodynamics of Substances with Simultaneously Negative Values oF ϵ and μ. Soviet Physics Uspekhi. 1968; 10(4): 509-514. doi: 10.1070/pu1968v010n04abeh003699
2. Pendry JB, Holden AJ, Robbins DJ, et al. Magnetism from conductors and enhanced nonlinear phenomena. IEEE Transactions on Microwave Theory and Techniques. 1999; 47(11): 2075-2084. doi: 10.1109/22.798002
3. Pendry JB, Holden AJ, Stewart WJ, et al. Extremely Low Frequency Plasmons in Metallic Mesostructures. Physical Review Letters. 1996; 76(25): 4773-4776. doi: 10.1103/physrevlett.76.4773
4. Marqués R, Martel J, Mesa F, et al. Left-Handed-Media Simulation and Transmission of EM Waves in Subwavelength Split-Ring-Resonator-Loaded Metallic Waveguides. Physical Review Letters. 2002; 89(18). doi: 10.1103/physrevlett.89.183901
5. Zheng H, Pham TS, Chen L, et al. Metamaterial Perfect Absorbers for Controlling Bandwidth: Single-Peak/Multiple-Peaks/Tailored-Band/Broadband. Crystals. 2023; 14(1): 19. doi: 10.3390/cryst14010019
6. Pendry J. Negative refraction. Contemporary Physics. 2004; 45(3): 191-202. doi: 10.1080/00107510410001667434
7. Abdulkarim YI, Mohanty A, Acharya OP, et al. A Review on Metamaterial Absorbers: Microwave to Optical. Frontiers in Physics. 2022; 10. doi: 10.3389/fphy.2022.893791
8. Almoneef TS, Ramahi OM. Metamaterial electromagnetic energy harvester with near unity efficiency. Applied Physics Letters. 2015; 106(15). doi: 10.1063/1.4916232
9. Góra P, Łopato P. Metamaterials' Application in Sustainable Technologies and an Introduction to Their Influence on Energy Harvesting Devices. Applied Sciences. 2023; 13(13): 7742. doi: 10.3390/app13137742

10. Nguyen TT, Lim S. Design of Metamaterial Absorber using Eight-Resistive-Arm Cell for Simultaneous Broadband and Wide-Incidence-Angle Absorption. Scientific Reports. 2018; 8(1). doi: 10.1038/s41598-018-25074-8

11. Pham TS, Zheng H, Chen L, et al. Wide-incident-angle, polarization-independent broadband-absorption metastructure without external resistive elements by using a trapezoidal structure. Scientific Reports. 2024; 14(1). doi: 10.1038/s41598-024-60171-x

12. Singh G, Ni R, Marwaha A. A Review of Metamaterials and its Applications. International Journal of Engineering Trends and Technology. 2015; 19(6): 305-310. doi: 10.14445/22315381/ijett-v19p254

13. Adepoju W, Bhattacharya I, Sanyaolu M, et al. Critical Review of Recent Advancement in Metamaterial Design for Wireless Power Transfer. IEEE Access. 2022; 10: 42699-42726. doi: 10.1109/access.2022.3167443

14. Rong C, Yan L, Li L, et al. A Review of Metamaterials in Wireless Power Transfer. Materials. 2023; 16(17): 6008. doi: 10.3390/ma16176008

15. Liao S, Qiao Z, Sui J, et al. Multifunctional Device for Circular to Linear Polarization Conversion and Absorption. Annalen der Physik. 2023; 535(7). doi: 10.1002/andp.202300195

16. Liao S, Sui J, Zhang H. Switchable ultra-broadband absorption and polarization conversion metastructure controlled by light. Optics Express. 2022; 30(19): 34172. doi: 10.1364/oe.472336

17. Guo Z, Gao C, Zhang H. Direction-Dependent Janus Metasurface Supported by Waveguide Structure with Spoof Surface Plasmon Polariton Modes. Advanced Materials Technologies. 2022; 8(2). doi: 10.1002/admt.202200435

18. Guo S, Hu C, Zhang H. Unidirectional ultrabroadband and wide-angle absorption in graphene-embedded photonic crystals with the cascading structure comprising the Octonacci sequence. Journal of the Optical Society of America B. 2020; 37(9): 2678. doi: 10.1364/josab.399048

19. Anwar S, Khan M. Simple design of metamaterial sensor for biomedical sensing. Physica Scripta. 2022; 97(12): 125504. doi: 10.1088/1402-4896/ac9a87

20. Fan J, Zhang L, Wei S, et al. A review of additive manufacturing of metamaterials and developing trends. Materials Today. 2021; 50: 303-328. doi: 10.1016/j.mattod.2021.04.019

21. Lu C, Huang X, Tao X, et al. Comprehensive Analysis of Side-Placed Metamaterials in Wireless Power Transfer System. IEEE Access. 2020; 8: 152900-152908. doi: 10.1109/access.2020.3017492

22. Hong Hiep LT, Pham TS, Khuyen BX, et al. Enhanced transmission efficiency of magneto-inductive wave propagating in non-homogeneous 2-D magnetic metamaterial array. Physica Scripta. 2022; 97(2): 025504. doi: 10.1088/1402-4896/ac4a3a

23. Hiep LTH, Khuyen BX, Tung BS, et al. Flexible Magnetic Metasurface with Defect Cavity for Wireless Power Transfer System. Materials. 2022; 15(19): 6583. doi: 10.3390/ma15196583

24. Wu Z, Yu H, Schreurs D, et al. Wireless power transfer based on 2D routing. Scientific Reports. 2022; 12(1). doi: 10.1038/s41598-022-22319-5

25. Zeng Y, Lu C, Liu R, et al. Wireless Power and Data Transfer System Using Multidirectional Magnetic Coupler for Swarm AUVs. IEEE Transactions on Power Electronics. 2023; 38(2): 1440-1444. doi: 10.1109/tpel.2022.3214318

26. Shamonina E, Kalinin VA, Ringhofer KH, et al. Magneto-inductive waveguide. Electronics Letters. 2002; 38(8): 371-373; doi: 10.1049/el:20020258

27. Shamonina E, Solymar L. Properties of magnetically coupled metamaterial elements. Journal of Magnetism and Magnetic Materials. 2006; 300(1): 38-43. doi: 10.1016/j.jmmm.2005.10.028

28. Liu W, Chau KT, Tian X, et al. Smart wireless power transfer—opportunities and challenges. Renewable and Sustainable Energy Reviews. 2023; 180: 113298. doi: 10.1016/j.rser.2023.113298

29. Bennia F, Boudouda A, Nafa F. Optimal design of wireless power transfer coils for biomedical implants using machine learning and meta-heuristic algorithms. Electrical Engineering. 2024. doi: 10.1007/s00202-024-02345-4

30. Celentano A, Paolino C, Pareschi F, et al. Mutual Inductance Measurement in Wireless Power Transfer Systems Operating in the MHz Range. IEEE Transactions on Circuits and Systems II: Express Briefs. 2024; 71(3): 1715-1720. doi: 10.1109/tcsii.2023.3334432

31. Hoang MK, Xuan TK, Xuan TP, et al. A Design of Magnetic Resonant Wireless Power Transfer System using Flexible Resonator Coils. Journal of Magnetics. 2023; 28(3): 323-330. doi: 10.4283/jmag.2023.28.3.323

32. Shah IA, Zada M, Shah SAA, et al. Flexible Metasurface-Coupled Efficient Wireless Power Transfer System for Implantable Devices. IEEE Transactions on Microwave Theory and Techniques. 2024; 72(4): 2534-2547. doi: 10.1109/tmtt.2023.3319050

33. Jo S, Lee W, Lee H. Metasurface Patch for Wireless Power Transfer in Implantable Devices. Advanced Functional Materials. 2023; 33(38). doi: 10.1002/adfm.202300027

34. Feis J, Solymar L, Shamonina E. Topological wireless communication in the stopband of magnetoinductive lines. Journal of Applied Physics. 2023; 133(22). doi: 10.1063/5.0146831

35. Voronov A, Sydoruk O, Syms RRA. Power waves and scattering parameters in magneto-inductive systems. AIP Advances. 2021; 11(4). doi: 10.1063/5.0049806

36. Pham TS, Khuyen BX, Tung BS, et al. Enhanced Efficiency of Asymmetric Wireless Power Transmission Using Defects in 2D Magnetic Metamaterials. Journal of Electronic Materials. 2020; 50(2): 443-449. doi: 10.1007/s11664-020-08586-w

37. Choi J, Seo C. High-Efficiency Wireless Energy Transmission Using Magnetic Resonance Based on Negative Refractive Index Metamaterial. Progress In Electromagnetics Research. 2010; 106: 33-47. doi: 10.2528/pier10050609

38. Hiep LTH, Bui HN, Tung BS, et al. Enhanced efficiency of magnetic resonant wireless power transfer system using rollable and foldable metasurface based on polyimide substrate. Applied Physics A. 2024; 130(7). doi: 10.1007/s00339-024-07684-4

39. Zhi Sun, Akyildiz IF. Magnetic Induction Communications for Wireless Underground Sensor Networks. IEEE Transactions on Antennas and Propagation. 2010; 58(7): 2426-2435. doi: 10.1109/tap.2010.2048858

40. Ranaweera ALAK, Duong TP, Lee JW. Experimental investigation of compact metamaterial for high efficiency mid-range wireless power transfer applications. Journal of Applied Physics. 2014; 116(4). doi: 10.1063/1.4891715

41. Aydin K, Ozbay E. Capacitor-loaded split ring resonators as tunable metamaterial components. Journal of Applied Physics. 2007; 101(2). doi: 10.1063/1.2427110

42. Pham TS, Bui HN, Lee JW. Wave propagation control and switching for wireless power transfer using tunable 2-D magnetic metamaterials. Journal of Magnetism and Magnetic Materials. 2019; 485: 126-135. doi: 10.1016/j.jmmm.2019.04.034